Frontal Circulations in the Presence of Small Moist Symmetric Stability

KERRY A. EMANUEL

Center for Meteorology and Physical Oceanography, Massachusetts Institute of Technology, Cambridge, MA 02139

(Manuscript received 11 May 1984, in final form 10 October 1984)

ABSTRACT

Observations in saturated frontal regions occasionally show that the flow has become neutral to reversible slantwise displacements along pseudo-angular momentum surfaces so that the effective potential vorticity is nearly zero for further saturated displacements. A strong response to frontogenesis is indicated in these regions, as suggested by the parabolic nature of the Sawyer–Eliassen equation when the potential vorticity vanishes. Using idealized distributions of temperature and geostrophic deformation, we derive solutions of the aforementioned equation for the cross-front circulation in the case where the potential vorticity is vanishingly small for upward displacements but moderate for downward displacements. While the solutions are self-consistent, it is not known whether they are unique. They show that a strong, concentrated sloping updraft occurs somewhat to the warm side of the region of maximum geostrophic compression of the isotherms. This circulation closely resembles the flow in a mesoscale precipitation band analyzed by Sanders and Bosart.

1. Introduction

Recent observations of frontal systems (e.g., Hobbs, 1978; Carbone, 1982) have revealed a great wealth of organized mesoscale precipitation bands. Some of the bands occur very close to the position of recognizable surface fronts, while others bear a less obvious relation to the latter. A variety of physical mechanisms has been proposed to explain bands of the latter kind, including ducted gravity waves (Lindzen and Tung, 1976) and conditional symmetric instability (Bennetts and Hoskins, 1979; Emanuel, 1983a,b). A review of the present state of understanding of these bands may be found in Parsons and Hobbs (1983).

One part of the New England Winter Storms Experiment was specifically designed to test the hypothesis that moist symmetric instability, hereafter referred to as slantwise moist convection, is responsible for the majority of bands observed in association with winter storms in New England. Detailed results of these experiments are forthcoming. We can state at this time, however, that a majority of those cases where bands were clearly observed was nearly neutral or slightly unstable to slantwise convection, as had been reported by Emanuel (1983b) for a case of banded precipitation in Oklahoma. The assessment of stability is based on the method outlined in the aforementioned paper. According to reversible parcel theory, a parcel is conditionally unstable to slantwise convection if it achieves positive buoyancy when reversibly lifted along a surface of constant geostrophic pseudo-angular momentum M, defined by

$$M \equiv V_g + fx,$$

where f is the Coriolis parameter, V_g the component of geostrophic wind along isotherms, and x a coordinate orthogonal to the isotherms and hence to V_g.

During the course of the experiment several attempts were made to fly an instrumented aircraft along a surface of constant M. This was done by estimating the position of M surfaces from cross sections constructed using standard rawinsonde soundings and then measuring M on board the aircraft, assuming that the measured V was close to the geostrophic value. In practice, however, V was observed to contain significant ageostrophic components, especially when strong bands were present. Nevertheless we were successful in completing flights over substantial distances where M departed only slightly from its initial value. A preliminary sounding of temperature and dew point along one such surface is presented in Fig. 1, with departures of M from its initial value indicated in parentheses. Note that over the constant M portion of the flight, which descended along the M surface, the sounding is close to moist adiabatic. We interpret this observation to imply that some form of slantwise moist convective adjustment has taken place, or is occurring at the time the observation is made. The theory developed by Emanuel (1983a,b) strongly suggests that such an adjustment is likely in an initially slantwise-unstable baroclinic atmosphere when lifted to saturation.

What comes as some surprise is that the bands should sometimes persist for many hours after the condition of neutrality is observed. This was the case, for example, with the snow bands observed during the storm of 11–12 February 1983 as reported by

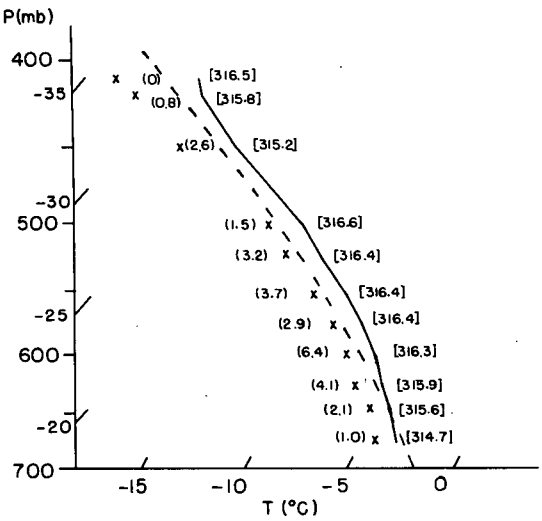

FIG. 1. Aircraft sounding along M surface around 0600 GMT 16 November 1983, between Brunswick, Maine and Portsmouth, New Hampshire. The solid line denotes temperature sounding; crosses show dew point temperature. Dashed line is a pseudo-moist adiabat. Numbers in parentheses to left of sounding show departure of M (m s^{-1}) from initial value, while numbers in brackets are equivalent potential temperature (K) with respect to ice processes.

Sanders and Bosart (1985). A clue as to why this might be the case occurs in their observation that some geostrophic deformation was acting on the large scale temperature gradient at the time that the band was present. As elementary considerations show that the response to frontogenetical forcing is inversely proportional to slantwise stability, a particularly strong response should ensue in an atmosphere which, having been previously unstable to slantwise convection, has undergone an adjustment to neutrality. It is the purpose of this paper to examine the nature of the response to frontogenetical forcing of an atmosphere which is nearly neutral to saturated slantwise convection.

2. Scaling of the Sawyer-Eliassen equation and validity of the geostrophic momentum approximation

By way of pursuing this problem we consider the response to geostrophic deformation of an idealized baroclinic zone in which the effective potential vorticity takes on one value for unsaturated (downward) motions and another in cloudy regions of ascent. The geostrophic potential vorticity is here defined

$$q_g \equiv \frac{g}{f\theta_0}[(f\hat{k} + \nabla \times \mathbf{V}_g)\cdot\nabla\theta], \tag{1}$$

where θ is the potential temperature with reference value θ_0, g the acceleration of gravity, f the Coriolis parameter (assumed constant), and $\mathbf{V}_g$ the geostrophic velocity vector. If we choose a coordinate system in such a way that θ varies only with x and z, the above may be written

$$q_g = N^2\left(1 + f^{-1}\frac{\partial V_g}{\partial x}\right) - \left(\frac{\partial V_g}{\partial z}\right)^2, \tag{2}$$

where N is the buoyancy frequency and V_g is the y component of the geostrophic wind. The thermal wind relation

$$\frac{g}{\theta_0}\frac{\partial\theta}{\partial x} = f\frac{\partial V_g}{\partial z}$$

has been used in deriving (2) from (1).

In saturated regions we additionally define a moist geostrophic potential vorticity:

$$q_{gw} \equiv N_w^2\left(1 + f^{-1}\frac{\partial V_g}{\partial x}\right) - \left(\frac{\partial V_g}{\partial z}\right)^2, \tag{3}$$

where N_w is a buoyancy frequency for moist adiabatic motions. As shown by Durran and Klemp (1982), N_w is related to the vertical gradient of equivalent potential temperature by

$$N_w^2 = \frac{g}{\theta_0}\frac{\Gamma_m}{\Gamma_d}\frac{\partial\theta_e}{\partial z},$$

where Γ_m and Γ_d are the moist and dry adiabatic lapse rates, respectively.

The geostrophic potential vorticity plays an extremely important role in the dynamics of frontal zones. When q_g is negative, the flow is symmetrically unstable, while when q_{gw} is negative in saturated regions of the atmosphere, while q_g is elsewhere positive, slantwise moist convection ensues (Bennetts and Hoskins, 1979; Emanuel, 1983a,b). As has been mentioned in the Introduction, there exists evidence that slantwise moist convection renders regions of the atmosphere neutral to further convection in which case q_{gw}, defined by (3), tends to zero from below.

When q_g and q_{gw} are everywhere positive, they determine the intensity of the vertical velocity forced by a given geostrophic deformation of the temperature field. This can be seen in the mathematical form of the Sawyer-Eliassen equation phrased in geostrophic coordinates. The latter are defined by the transformations

$$X \equiv x + V_g/f,$$
$$Z \equiv z, \tag{4}$$

where V_g is again the front-parallel component of the geostrophic flow. In these coordinates, the Sawyer-Eliassen equation takes the form (e.g., Hoskins and Draghici, 1977)

$$\frac{\partial}{\partial X}\left(q_g\frac{\partial\psi}{\partial X}\right) + f^2\frac{\partial^2\psi}{\partial Z^2} = 2Q, \tag{5}$$

where ψ is the streamfunction in the plane across the front, which is taken to be parallel to the y axis, and Q is the geostrophic forcing,

$$Q \equiv f\left(\frac{\partial V_g}{\partial X}\frac{\partial U_g}{\partial Z} - \frac{\partial U_g}{\partial X}\frac{\partial V_g}{\partial Z}\right),$$

where U_g is the cross-front geostrophic flow.

One can see immediately that q_g determines the ellipticity of the Poisson equation (5): If q_g is positive it is elliptic while if q_g is negative it is hyperbolic. In the latter case, the assumptions in the derivation of (5) are invalid and the resulting flow will contain a large convective component. As we shall show presently, q_g must be sufficiently large for validity of the geostrophic momentum approximation involved in the derivation of (5).

If in a particular circumstance q_g is constant in the region of interest, then we may scale Z by H and X by the quantity $Hq_g^{1/2}/f$ where H is a characteristic depth, whence (5) takes the form

$$\nabla^2\psi = 2H^2f^{-2}Q. \tag{6}$$

The amplitude of the streamfunction is thus determined purely by H and the geostrophic forcing Q. The vertical velocity, however, will scale as $q_g^{-1/2}$:

$$w = \frac{\partial\psi}{\partial x} = \frac{\eta_g}{f}\frac{\partial\psi}{\partial X^*} = \frac{\eta_g}{Hq_g^{1/2}}\frac{\partial\psi}{\partial X},$$

where η_g is the geostrophic absolute vorticity and the asterisk denotes the unscaled value of X. Thus a large response in vertical motion may be expected in regions where q_g is small and Q is large.

It is evident that in the limit of small q_g the ageostrophic velocities blow up and one is led to question the realism of the solutions from two points of view. The first concerns the validity of the geostrophic momentum approximation used in deriving (5), while the second has to do with the likelihood of the development of turbulence. Both concerns lead to similar restrictions on the smallness of the potential vorticity.

The geostrophic momentum approximation formally asserts that the total acceleration of the ageostrophic velocities is small compared to that of the geostrophic velocities. The approximation is based on the observed smallness of a Rossby number based on Lagrangian time scales rather than on Eulerian length and velocity scales and leads to an energetically consistent set of equations (see Hoskins, 1975, for an extensive review of the geostrophic momentum equations).

An estimate can be made of the conditions for the validity of the geostrophic momentum approximation simply by using the scaling of length and streamfunction evident in (6). Consider a north-south two-dimensional frontal zone subject to a constant geostrophic stretching deformation. We may represent the horizontal velocities and pressure by

$$U = U_g' - \alpha x + U_{ag},$$
$$V = V_g' + \alpha y + V_{ag},$$
$$p = p' + \rho_0 f\alpha xy - \tfrac{1}{2}\rho_0\alpha^2(x^2 + y^2),$$

where 2α is the magnitude of the deformation, ρ_0 is a reference density, U_g' and V_g' are departures of the geostrophic velocities from those represented by the simple deformation field, and U_{ag} and V_{ag} are ageostrophic velocities. Hoskins and Bretherton (1972) showed that all variables aside from the basic deformation flow and associated pressure field are independent of y so that $U_g' = 0$. The zonal momentum equation may be written

$$\frac{dU_g}{dt} + \frac{dU_{ag}}{dt} = -\frac{1}{\rho_0}\frac{\partial p}{\partial x} + fV.$$

Using $U_g = -\alpha x$ for the first term on the left and substituting the previous expressions for u, v and p; we have

$$\frac{dU_{ag}}{dt} - \alpha(U_{ag} - \alpha x) = -\frac{1}{\rho_0}\frac{\partial p'}{\partial x} - f\alpha y + \alpha^2 x + f(V_g' + V_{ag} + \alpha y),$$

which reduces to

$$\frac{dU_{ag}}{dt} - \alpha U_{ag} = -\frac{1}{\rho_0}\frac{\partial p'}{\partial x} + fV', \tag{7}$$

where $V' \equiv V_g' + V_{ag}$.

According to (7), we may assume geostrophic balance of the perturbation pressure gradient and meridional flow if

$$|U_{ag}| \ll |f\alpha^{-1}V'|, \tag{8}$$

$$\left|\frac{dU_{ag}}{dt}\right| \ll |fV'|. \tag{9}$$

The magnitudes of the terms on the left of (8) and (9) are now estimated from the scaling of the streamfunction equation (6) with constant potential vorticity. According to (6), the magnitude of ψ will be

$$\psi \sim Q_0 f^{-2}H^2, \tag{10}$$

where H is a vertical length scale and Q_0 is a scale for Q which, from the latter's definition, will be of order

$$Q_0 \sim f\alpha V_{z0}, \tag{11}$$

where V_{z0} is a typical value of the vertical shear. Using the coordinate transformations (4) and the chain rule,

$$U_{ag} = -\frac{\partial\psi}{\partial z} = -\frac{\partial\psi}{\partial Z} - f^{-1}\frac{\partial V_g}{\partial z}\frac{\partial\psi}{\partial X^*}.$$

Scaling X^* by $Hq^{1/2}f^{-1}$ as before and using (10) and (11) in the above expression, we have

$$U_{ag} = O(\alpha f^{-1}V_{z0}H) + O(\alpha V_{z0}^2 f^{-1}Hq^{-1/2}). \tag{12}$$

The magnitude of the acceleration of U_{ag} is similarly estimated:

$$\frac{dU_{ag}}{dt} \sim U_g \frac{\partial U_{ag}}{\partial X^*} + w \frac{\partial U_{ag}}{\partial Z^*}$$
$$= O(U_g \alpha V_{z0}^2 q^{-1}) + O(\eta_0 \alpha^2 V_{z0}^3 H f^{-2} q^{-1}), \quad (13)$$

where η_0 is an absolute vorticity scale.

Using (12) and (13), the inequalities (8) and (9) result in the four requirements

$$1 \gg \frac{\alpha^2}{f^2}, \quad (14)$$

$$\frac{q}{V_{z0}^2} \gg \frac{\alpha^4}{f^4}, \quad (15)$$

$$\frac{q}{V_{z0}^2} \gg \frac{\alpha U_g}{f V_{z0} H}, \quad (16)$$

$$\frac{q}{V_{z0}^2} \gg \frac{\eta_0 \alpha^2}{f^3}. \quad (17)$$

If we also take $U_g = \alpha x \sim \alpha V_z H f^{-1}$, then (16) and (17) are virtually identical. In view of (14), it is evident that (16) and (17) are stronger conditions on q than is (15). Thus, in addition to the requirement that the magnitude of the geostrophic deformation be small compared to f (which is usually observed to be the case), we will use (17) as a restriction on the smallness of q. Note that since both V_z and η_g become large near the front, (17) is eventually violated as frontogenesis proceeds.

In addition to the aforementioned requirements for the validity of the geostrophic momentum approximation, we must also be sure that the stability is large enough to prevent Kelvin-Helmholtz instability and subsequent turbulent breakdown. For the flow to remain stable in this sense, it is sufficient that the Richardson number (Ri) remain greater than ¼. From the definition (2) of q, this may be stated

$$\mathrm{Ri} = \frac{f}{\eta}\left(\frac{q}{V_z^2} + 1\right) > \frac{1}{4},$$

or

$$\frac{q}{V_z^2} > \frac{1}{4}\frac{\eta}{f} - 1, \quad (18)$$

where η is the absolute geostrophic vorticity. Provided that $\eta < 4f$, (17) will be a stronger condition on q than (18). The expressions (14), (17) and (18) may be considered fundamental requirements for the validity of the geostrophic momentum approximation.

3. The cross-stream circulation in an idealized partly saturated frontal zone

As a means of determining some of the elementary aspects of the effects of condensation on frontal circulations, we will solve the cross-stream circulation equation (5) with specified geostrophic wind and deformation characteristic of a front, while letting q take on one value in unsaturated regions, and another effective value, q_w, where liquid water is present. In order to make progress while retaining simplicity, it is necessary to make some rather restrictive assumptions. The first is that the circulation has evolved in such a way that regions of upward motion are saturated while elsewhere the flow is unsaturated. This presumes, of course, that all condensed water immediately falls out and we will further assume that it does so without evaporating appreciably. This may be approximately true with respect to snow and in other cases may be regarded as a crude approximation of nature.

With these assumptions, the potential vorticity formally becomes a function of ψ and (5) becomes nonlinear. To circumvent this problem, we first *assume* that upward motion prevails for all X greater than some value L, while downward motion occurs elsewhere. Having then found a solution to (5), we adjust L toward the value of X where w changes sign and so attempt to iterate toward a self-consistent solution of (5). Even if we are successful in this endeavor, however, there is no guarantee that the solution is unique; one might very well have postulated a number of spatially discrete regions of small q instead and converged on a different self-consistent solution. We take the position that some of the salient features of the effects of condensation will be illustrated adequately by the self-consistent solution we do obtain, even if other self-consistent solutions might have been attained through an initial value approach to the same problem.

In order to obtain more or less realistic solutions to (5), we choose a forcing which is concentrated at $X = 0$ and which decays away exponentially at large $|X|$:

$$Q = Q_0 e^{-b|X|}. \quad (19)$$

This may be regarded as pertaining to a situation in which the geostrophic deformation and/or the horizontal temperature gradient decay exponentially away from $X = 0$. If the geostrophic deformation varies with X and if $\partial V_g/\partial Z$ is not zero, then it follows that U_g is a function of Z as well as X and we must therefore account for the shearing deformation term in the geostrophic forcing, unless $\partial V_g/\partial X$ is zero.

In summary, (5) will be solved for the case where Q is given by (19) and in which $q_g = q_1$ for $X > L$ and $q_g = q_2$ for $X \leq L$. The assumption that w changes sign along a surface of nearly constant X will be justified *a posteriori*. We also assume that the domain is bounded above and below by rigid plates separated by a distance H; since (5) is elliptic for positive q the artificial upper lid will have only quantitative effects on the solution away from the upper boundary. The basic state which will be used

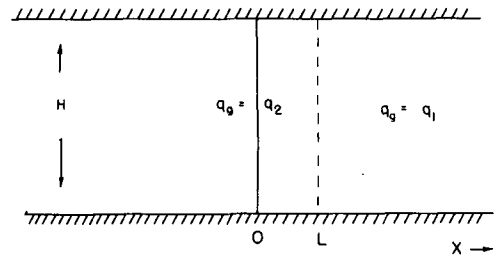

FIG. 2. Assumed distribution of q_g in X–Z space used to calculate the cross-front circulation. Upward motion is assumed for $X > L$, where $q_g = q_1^*$, while downward motion is assumed elsewhere, where $q_g = q_2^*$. The geostrophic forcing is greatest along $X = 0$.

to determine the cross-front flow is illustrated in Fig. 2.

Before solving (5), it proves convenient to normalize the dependent and independent variables as follows:

$$\left.\begin{aligned} X^* &\equiv Hq_2^{*1/2}f^{-1}\pi^{-1}X \\ Z^* &\equiv HZ \\ \psi^* &\equiv 2\pi^{-3}f^{-2}Q_0H^2\psi \\ b^* &\equiv H^{-1}q_2^{*-1/2}f\pi b \\ q_1^* &\equiv q_2^*q_1 \end{aligned}\right\}, \tag{20}$$

where the asterisks denote the dimensional variables. With these normalizations, (5) becomes

$$\pi^2\frac{\partial}{\partial X}\left(\tilde{q}\frac{\partial\psi}{\partial X}\right)+\frac{\partial^2\psi}{\partial Z^2}=\pi^3e^{-b|X|}, \tag{21}$$

with

$$\tilde{q}=\begin{cases}q_1, & X>L\\ 1, & X\leqslant L.\end{cases}$$

The boundary conditions on ψ are

$$\begin{aligned}&\psi=0 \quad \text{on} \quad Z=0,\ 1;\\ &\psi=0 \quad \text{as} \quad |X|\to\infty.\end{aligned} \tag{22}$$

We solve (21) independently in the regions $X > L$, $0 < X < L$ and $X < 0$ and match the solutions across $X = L$ and $X = 0$. The matching conditions are

$$\begin{aligned}&\psi,\ \tilde{q}\frac{\partial\psi}{\partial X} \text{ continuous across } X=L,\\ &\psi,\ \frac{\partial\psi}{\partial X} \text{ continuous across } X=0.\end{aligned} \tag{23}$$

In each region, the solution is represented by series of the form

$$\sum_n J_n(X)\sin(n\pi Z),$$

which satisfy the conditions on ψ at $Z = 0$, 1. Here the J_n are as yet undetermined functions of X. We find the following solutions which satisfy the boundary conditions (22) and the matching conditions (23):

$$X>L:\quad \psi=\sum_{\text{odd}}(F_ne^{-bX}+A_ne^{-r_nX})\sin(n\pi Z), \tag{24}$$

$$X\leqslant L:\quad \psi=\sum_{\text{odd}}\left[G_n\left(e^{-b|X|}-\frac{b}{n}e^{-n|X|}\right)+C_ne^{nX}\right]\sin(n\pi Z),$$

where the summations are taken over odd n only and the coefficients are defined

$$\left.\begin{aligned} F_n &\equiv \frac{4}{n(b^2q_1-n^2)}\\ G_n &\equiv \frac{4}{n(b^2-n^2)}\\ A_n &\equiv e^{r_nL}\left[\frac{G_n[b(e^{-bL}-2e^{-nL})+ne^{-bL}]-F_ne^{-bL}(q_1b+n)}{q_1r_n+n}\right]\\ C_n &\equiv e^{-nL}\left[A_ne^{-r_nL}+F_ne^{-bL}+G_n\left(\frac{b}{n}e^{-nL}-e^{-bL}\right)\right]\\ r_n &\equiv nq_1^{-1/2}\end{aligned}\right\}.$$

Once a solution (24) is found it is checked for self-consistency in the sense that upward motion should occur where $q = q_1$, with downward motion elsewhere. If this is not the case, L is adjusted toward the region where w is observed to change sign. By iterating in this fashion, a nearly (but not perfectly) self-consistent solution was always found. We take this to imply that the surface along which w actually changes sign is very nearly, but not exactly, a surface of constant X. Indeed, since (24) is not separable, there is no reason why $w = 0$ must lie along X = constant. In order to test the assumption, solutions representing a ten-term truncation of (24) were examined over a

small interval of X near $X = L$. We find that the line along which w actually changes sign varies no more than 0.02 nondimensional units in X, so that the assumption that w vanishes along a line of constant X is excellent, though not exact. An extremely good approximation to L can be found, it turns out, by demanding that $\partial\psi/\partial X$, as represented by the *first term only* of (24), vanish at $X = L$. This results in the following condition on L:

$$L \cong \frac{1}{b-1}\ln\left[1 + \frac{(1-q_1^{1/2})(b-1)}{2(1+bq_1^{1/2})}\right]. \quad (25)$$

When $q_1 = 1$, which denotes uniform potential vorticity throughout the domain, $L = 0$ as we expect from symmetry. When $q_1 < 1$, L is positive definite (and continuous and finite through $b = 1$). In the limit of small q_1,

$$L \simeq \frac{1}{b-1}\ln\left(\frac{1+b}{2}\right), \quad q_1 \ll 1. \quad (26)$$

This value of L is plotted as a function of the parameter b, which measures the decay of the forcing away from $X = 0$, in Fig. 3. The maximum value of L, which is ln2, is attained when $b = 0$ while L becomes vanishingly small with large b.

It was found that a three- or four-term approximation of the solution (24) is virtually indistinguishable from solutions which retain more terms. All the solutions presented here represent truncations of (24) to six terms, with L approximately determined from (25).

The solution for the streamfunction when $q_1 = 1$ and $b = 5.1$ is plotted in physical space for the case V_z = constant in Fig. 4. This is a classical picture of a frontal circulation, with upward motion to the right and downward motion to the left of the region of maximum geostrophic compression of the isotherms.

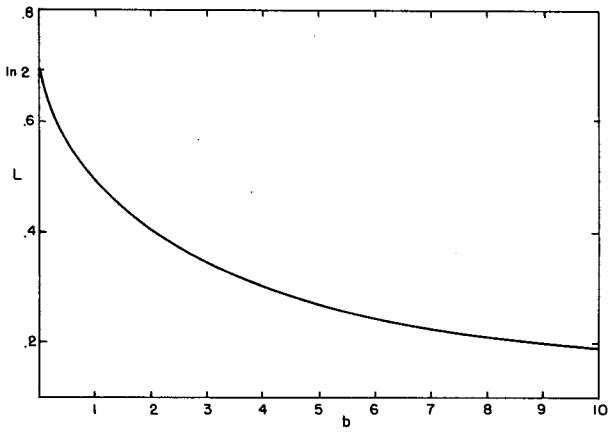

FIG. 3. The value of L when q_1 is small, according to (26), as a function of the rate of decay b of the geostrophic forcing away from $X = 0$.

By contrast, Fig. 5 shows the frontal circulation with q_1 reduced to 10^{-2}. As indicated by (25) or (26), the streamfunction maximum and the sloping updraft are displaced substantially toward the warm air and the latter is extremely concentrated, while the downward motion occurs over a considerably larger area. Figure 6 shows the same solution, but in this case we have assumed that the geostrophic vertical shear falls off as $e^{-b|X|}$, i.e.,

$$\frac{\partial V_g}{\partial z} = V_{z0}e^{-b|X|} = V_{z0}e^{-b^*|X^*+V_g/f|}.$$

This form of $\partial V_g/\partial z$ still implies some spatial variation of the background geostrophic deformation, since

$$\frac{\partial V_g}{\partial z} \neq \frac{\partial V_g}{\partial Z},$$

but the variation will not be as rapid as when $\partial V_g/\partial Z$ is constant.

A solution to the above is

$$X > 0: \quad V = \ln[C(x) + V_{z0}(z - z_0) + 1] - bx,$$
$$X < 0: \quad V = -\ln[-C(x) - V_{z0}(z - z_0) + 1] - bx, \quad (27)$$

where we have normalized V, b, x and z as follows:

$$\left.\begin{aligned} V_g^* &\equiv fb^{*-1}V \\ b^* &\equiv H^{-1}q_2^{*-1/2}f\pi b \\ x^* &\equiv Hq_2^{*1/2}f^{-1}\pi^{-1}x \\ z^* &\equiv Hz \end{aligned}\right\},$$

where the asterisks denote dimensional quantities. The arbitrary function $C(x)$ determines the x dependence of V. As a simple example, we choose $C(x) = 2\sinh bx$, which leads to $V \to 0$ as $|x| \to \infty$. This form of V is shown in Fig. 7. In both Figs. 6 and 7 we take $b = 5.1$ and $V_{z0} = 30.0$.

It should be noted that in the region of small q, the condition (17) for the validity of the geostrophic momentum approximation restricts the value of the forcing relative to q. From the definition of Q,

$$Q^* \sim f\alpha V_{z0}e^{-b|X|},$$

so that in the region where $q_g = q_1^*$, (17) may be written

$$q_1^* \gg Q^2f^{-4} \sim Q_0^2f^{-4}e^{-2bL}.$$

Using the normalized value of q^* from (20), the above may be written

$$Q_0 \ll f^2(q_1q_2^*)^{1/2}e^{bL}.$$

Thus for small q_1, the solutions are valid only when the magnitude of the forcing is sufficiently small. This can also be interpreted as a restriction on the magnitude of the (dimensional) streamfunction. From

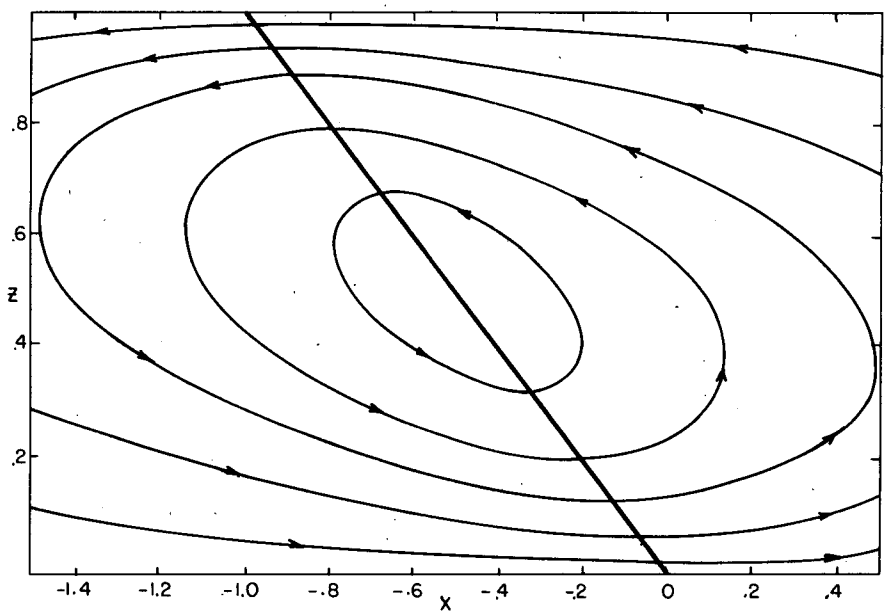

FIG. 4. The cross-front circulation in physical space for the case that $q_1 = 1.0$ and $b = 5.1$. The minimum value of the dimensionless streamfunction is -0.611; contours are at 0.1, 0.3, 0.5, 0.7, and 0.9 times the minimum value. The background dimensionless shear equals b. Heavy solid line denotes the position of the $X = 0$ surface.

(20), we may write using the preceding expression for Q_0

$$|\psi^*| \ll 2\pi^{-3}(q_1 q_2^*)^{1/2} H^2 e^{bL} |\psi|,$$

where the last coefficient is the magnitude of the dimensionless streamfunction. Taking $q^* = 10^{-4}$ s^{-2}, $q_1 = 10^{-2}$, and $H = 10$ km; and using the magnitude of the dimensionless streamfunction from Fig. 5, we have

$$|U^*| \sim |2\psi^* H^{-1}| \lessapprox 6 \text{ m s}^{-1}.$$

The above may be taken to be a restriction on the typical magnitude of ageostrophic U^* in the cold air; obviously much higher values of U^* will occur locally

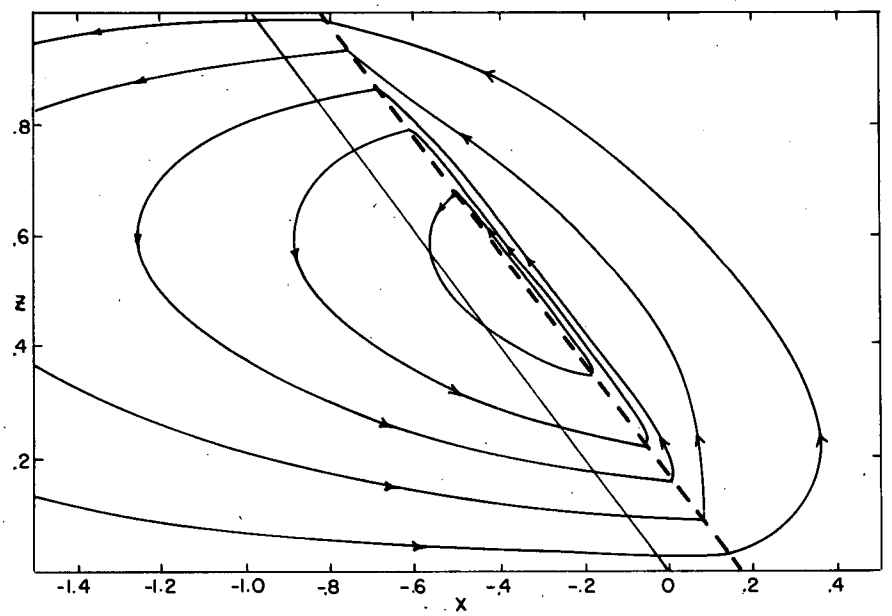

FIG. 5. As in Fig. 4 but for $q_1 = 10^{-2}$. The minimum value of the streamfunction is -1.769 in this case and the heavy dashed line denotes the surface $X = L$.

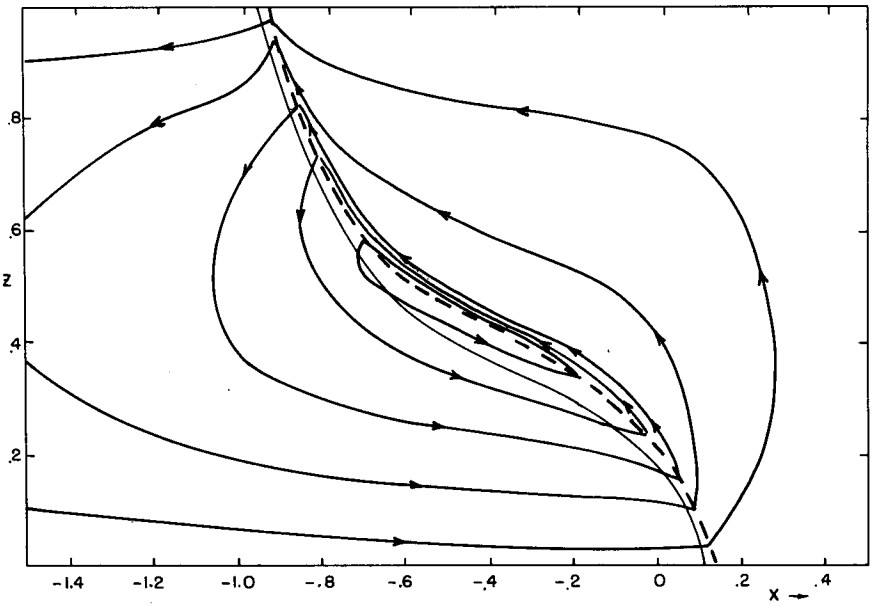

FIG. 6. Same circulation as depicted in Fig. 5, but where, in transforming to physical coordinates, we have taken a background V given by (27), with $C(x) = 2\sinh bx$, $V_{z0} = 30.0$, and $z_0 = 0.35$.

in the slanting jet. As q_1 becomes vanishingly small, the geostrophic momentum approximation breaks down and the inertia of the ageostrophic flow will become an important physical effect.

4. Discussion

The main result of the previous section is that in the limit of small moist potential vorticity, pressing the limits of validity of the geostrophic momentum equations, frontal forcing results in a strong, concentrated, sloping updraft which is located *ahead* of the region of maximum geostrophic frontogenetical forcing. From Fig. 3 and the scaling (20) it is evident that the distance between the "front" and the updraft will, in the atmosphere, have a typical value of order 50–200 km.

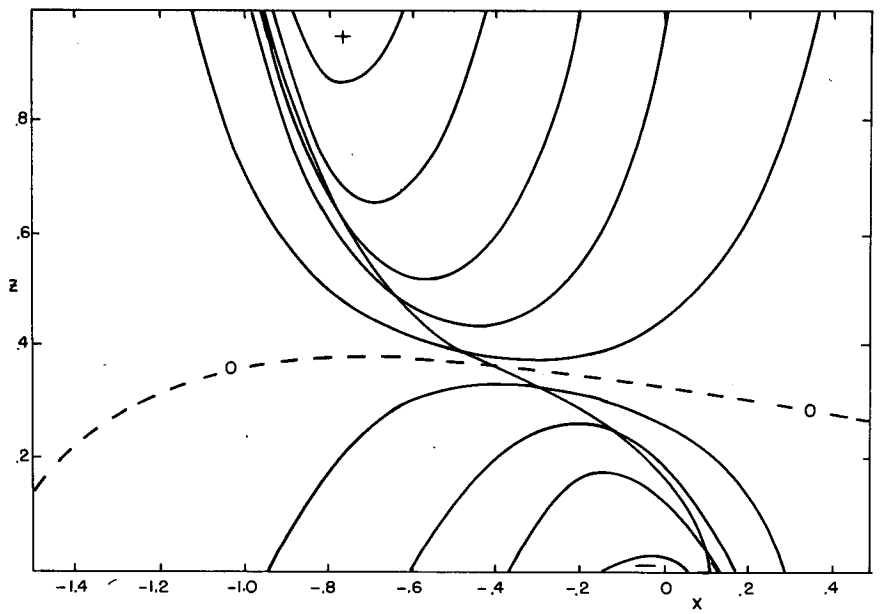

FIG. 7. Background V as given by (27) and used to construct Fig. 6. Contour intervals are 0.1, 0.3, 0.5, 0.7 and 0.9 times the maximum value; dashed line denotes $V = 0.0$.

The question naturally arises as to whether a diagnostic solution such as that displayed in Fig. 5 or Fig. 6 really represents, at least qualitatively, a solution which might have been arrived at through an initial value approach starting with very simple conditions. Close inspection of Fig. 5 or Fig. 6 reveals the seriousness of this question. The ageostrophic flow is slightly frontolytic at the position of the surface front, and strongly frontogenetic near the base of the sloping updraft. The implication is that the surface front will propagate more rapidly into the warm air than it would in the absence of condensation. It would also appear from these solutions that condensation may actually inhibit frontogenesis since the ageostrophic flow is frontolytic in the region of strongest temperature gradient. If, as the solutions presented here seemed to suggest, the ageostrophic convergence always occurs ahead of the strongest temperature gradient, with divergence in the vicinity of the strong gradients, then the collapse to discontinuity predicted in the dry case (Hoskins and Bretherton, 1972) may not occur. On the other hand, some of these speculations depend on the details of the temperature distribution at the surface. It would seem that these points are worth investigating with an initial value approach such as a numerical model.

Another effect which has been neglected here is evaporation or melting of falling precipitation. The form of the solutions evident in Figs. 5 and 6 suggest that evaporation will likely occur in the downdraft below the $w = 0$ surface, thus modifying the solution in the direction of a stronger downdraft near the front. Since the evaporation time scale may be much less than a pendulum day, a structure more like a density current may form and this would require full use of the primitive equations. If the precipitation is in frozen form, as it was in the New England band studied by Sanders and Bosart (1985), this is less likely to be a significant effect.

Once condensation begins in a frontal zone it would appear that sharp gradients in potential vorticity develop very rapidly. It is quite likely that these will be associated with local reversals of the potential vorticity gradient along θ surfaces; this raises the possibility of local barotropic or baroclinic instability in the frontal system. The general question of the stability of frontal zones to three-dimensional perturbations is quite broad and, it would seem, full of possibilities. Some of these have been examined recently by Mechoso and Sinton (1983), and are considered beyond the scope of the present work.

An example of a frontal circulation in the presence of small moist symmetric stability may be found in the work of Sanders and Bosart (1985) who examined, among other things, mesoscale bands which were observed in the snowstorm of 11–12 February 1983. A field of streamfunction computed from the ageostrophic horizontal flow in their cross section through

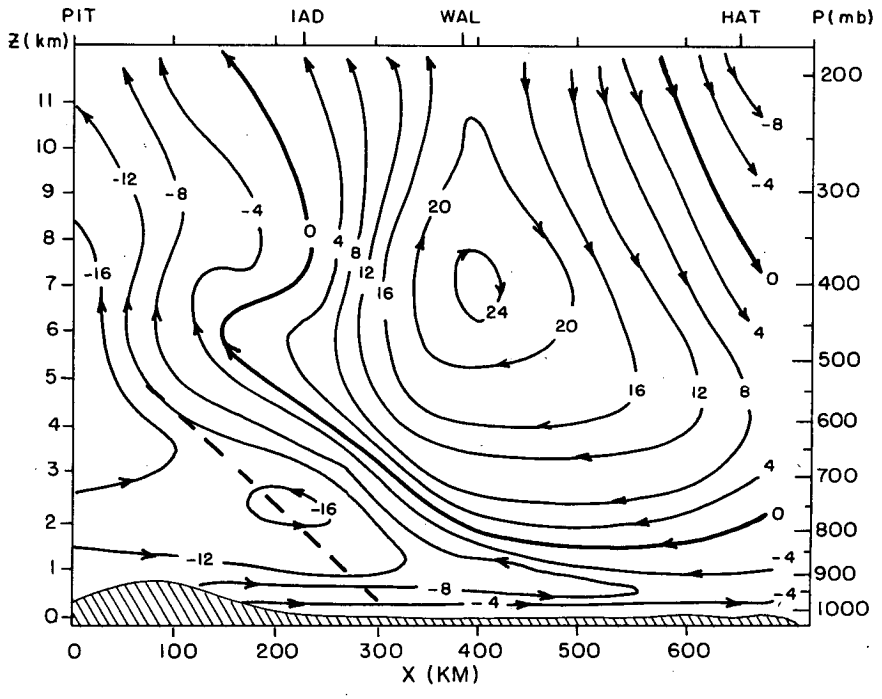

FIG. 8. The ageostrophic mass streamfunction (10^2 m mb s^{-1}) at 1200 GMT 11 February 1983, in a vertical plane from Pittsburgh, Pennsylvania to Cape Hatteras, North Carolina. Heavy dashed line shows axis of maximum frontogenetical forcing, $\partial U_g/\partial x \cdot \partial T/\partial x$. See Sanders and Bosart (1985) for details.

the bands is shown in Fig. 8, together with an indication of the axis of maximum frontogenesis. The streamlines reveal a concentrated sloping updraft located about 100 km ahead of the region of maximum forcing. Examination of cross sections of pseudo-angular momentum and equivalent potential temperature in Sanders and Bosart (1985) indeed show that the moist symmetric stability was small in the warm air in this case. The ageostrophic circulation shown in Fig. 8 qualitatively resembles the idealized flow in Figs. 5 and 6. We note that the cold air into which precipitation was falling was observed at times to be saturated, but in this case even the moist symmetric stability was large within the cold air.

5. Conclusions

Recent analyses of data from standard observing networks and from special field experiments reveal that lapse rates along pseudo-angular momentum surfaces in frontal zones are often moist adiabatic, suggesting that some kind of slantwise convective adjustment has taken place. The effective potential vorticity in these regions is very small. The analysis presented here shows that when such regions are subjected to frontogenetical forcing, a large response ensues on the warm side of the region of maximum forcing. If the potential vorticity is not small in the region of downward motion, as will be the case when such regions are unsaturated, the response takes the form of a concentrated sloping updraft ahead of the axis of maximum forcing, with weak downward motion elsewhere. The results suggest that condensation may inhibit frontogenesis under these conditions. The solutions compare favorably with the circulation in the baroclinic zone of an intense snowstorm analyzed by Sanders and Bosart (1985). Since condensation produces a strong source of potential vorticity at low levels, it is likely that the necessary condition for barotropic/baroclinic instability will be met locally in the frontal zone, possibly leading to waves of the type observed by Carbone (1982). Although the results presented here show the salient features of the response to frontogenesis of a flow with small moist slantwise stability, an initial value approach to the problem will be needed to determine the time-dependent characteristics of frontal circulations in the presence of slantwise moist convection.

Acknowledgments. In the course of this work, the author profited from numerous discussions with Frederick Sanders of M.I.T., Lance Bosart of SUNY–Albany and Alan Thorpe of the University of Reading, England. The work was completed with the assistance of grants ATM-8313454 and ATM-8209375 from the National Science Foundation.

REFERENCES

Bennetts, D. A., and B. J. Hoskins, 1979: Conditional symmetric instability—a possible explanation for frontal rainbands. *Quart. J. Roy. Meteor. Soc.*, **105,** 945–962.

Carbone, R. E., 1982: A severe frontal rainband. Part I: Stormwide hydrodynamic structure. *J. Atmos. Sci.*, **39,** 258–279.

Durran, D. R., and J. B. Klemp, 1982: On the effects of moisture on the Brunt-Väisälä frequency. *J. Atmos. Sci.*, **39,** 2152–2158.

Emanuel, K. A., 1983a: The Lagrangian parcel dynamics of moist symmetric instability. *J. Atmos. Sci.*, **40,** 2368–2376.

——, 1983b: On assessing local conditional symmetric instability from atmospheric soundings. *Mon. Wea. Rev.*, **111,** 2016–2033.

Hobbs, P. V., 1978: Organization and structure of clouds and precipitation on the mesoscale and microscale in cyclonic storms. *Rev. Geophys. Space Phys.*, **16,** 741–755.

Hoskins, B. J., 1975: The geostrophic momentum approximation and the semi-geostrophic equations. *J. Atmos. Sci.*, **32,** 233–242.

——, and F. P. Bretherton, 1972: Atmospheric frontogenesis models: Mathematical formulation and solution. *J. Atmos. Sci.*, **29,** 11–37.

——, and I. Draghici, 1977: The forcing of ageostrophic motion according to the semi-geostrophic equations and in an isentropic coordinate model. *J. Atmos. Sci.*, **34,** 1859–1867.

Lindzen, R. S., and K. K. Tung, 1976: Banded convective activity and ducted gravity waves. *Mon. Wea. Rev.*, **104,** 1602–1617.

Mechoso, C. R., and D. M. Sinton, 1983: On the energy analysis of the two-layer frontal model. *J. Atmos. Sci.*, **40,** 2069–2074.

Parsons, D. B., and P. V. Hobbs, 1983: The mesoscale and microscale structure and organization of clouds and precipitation in midlatitude cyclones. XI: Comparisons between observational and theoretical aspects of rainbands. *J. Atmos. Sci.*, **40,** 2377–2397.

Sanders, F., and L. Bosart, 1985: Mesoscale structure in the megalopolitan snowstorm of 11–12 February 1983. *J. Atmos. Sci.*, **42,** 1050–1061.